Correlated Segmental Dynamics in Amorphous Atactic Polystyrene: A Molecular Dynamics Simulation Study

Alexey V. Lyulin,*,† Nikolaj K. Balabaev,‡ and M. A. J. Michels†

Group Polymer Physics, Department of Applied Physics and Dutch Polymer Institute, Technische Universiteit Eindhoven, P.O. Box 513, 5600 MB Eindhoven, The Netherlands; and Institute of Mathematical Problems of Biology, Pushchino, 142290 Russia

Received July 30, 2002; Revised Manuscript Received October 1, 2002

ABSTRACT: Molecular dynamics simulations of bulk atactic polystyrene have been performed in a temperature range from 100 to 650 K at atmospheric pressure. Local translational mobility has been investigated by measuring the mean square translational displacements of monomers. The long-time asymptotic slope of these dependencies is 0.54 at $T > T_g$, showing Rouse behavior. Crossover from motion in the cage to Rouse-like dynamics has been studied at $T > T_g$ with a characteristic crossover time follows a power law behavior as a function of T, as predicted by mode-coupling theory (MCT). We studied the coherent intermediate scattering function and show the agreement with scaling predictions of MCT. Local orientational mobility has been studied via the orientational autocorrelation functions, ACFs (Legendre polynomials of the first and second order), of both the main-chain and side-group bonds. The ACF relaxation times analysis shows strong coupling between the phenyl groups and the backbone relaxation. The relaxation times of the orientational α-relaxation follow the same power law ($\gamma \sim 2.9$) as the characteristic translational diffusion time and the intermediate scattering function. Below T_g, both types of dynamics are described by the same activated law. The ACFs time-distribution functions reveal the existence of activated local rearrangements already above T_g.

1. Introduction

Investigation of local dynamical properties of amorphous polymers has been a subject of many studies, both experimental[1−16] and by means of computer simulation.[17−31] Nevertheless, questions concerning mechanisms of segmental mobility in the vicinity of the glass transition still remain open. Dynamical characteristics of amorphous polymers in the glassy state control such important properties as ductility, toughness, and impact resistance. It has recently become clear that the yield behavior of amorphous polymers is intimately linked to collective segmental dynamics of individual or neighboring chains.[3] Amorphous atactic polystyrene (PS) is, without a doubt, one of the most important examples of a widely used industrial plastic and a classical example of a mechanically brittle polymer (in contrast to polycarbonate, for example). It suits perfectly the study of the connection between local chemical and physical microstructure and global mechanical behavior.

Rotational oscillations of the backbone segments as well as side groups are the most general among different relaxation mechanisms in amorphous polymers, and PS is not an exception. Relaxational processes in amorphous PS in the vicinity of T_g have been studied experimentally by dynamic mechanical,[1−3] quasielastic neutron scattering,[4,5] dielectric,[6−12] and NMR techniques.[13−16] It is an established fact that above the PS glass-transition temperature ($T_g = 373$ K), the α-relaxation is the primary relaxation process of collective segmental motion,[32] and the temperature dependence of the characteristic relaxation times is well described by WLF equation.[33] Immediately below (when decreasing temperature) the primary relaxation, there is another, so-called β process, which appears in both dynamic mechanical and dielectric experiments. Different opinions about the nature of the β-relaxation exist. Usually this process is attributed to the rotational vibration of backbone segments,[2] but some authors have assigned the β process to the rotations of side phenyl groups.[13] The β peak merges into the α peak at high frequencies.[2] Mechanical-relaxation[1] and NMR experiments[14] revealed additional γ and δ processes associated with oscillatory motions of the side phenyl groups. Quasielastic neutron scattering experiments[5] reveal also the existence of a rather fast relaxation process on the picosecond scale in the temperature range covering the glass-transition temperature. This process was associated by the authors to librational motion of phenyl rings coupled with main-chain motion near T_g. Strong coupling of the side groups and backbone relaxation was found by Mansour et al.,[9,10] who studied dielectric relaxation of different chemical groups (*p*-cyanobenzyl, *p*-cyanobiphenyl) chemically fixed at the end of the PS chain or attached as side groups.

Not only the fast librational motions of side phenyl groups but also the slow π-flips of phenyl rings have been a subject of experimental and theoretical investigations. NMR experiments of Spiess[15,16] estimated the characteristic time of such flips as $\sim 10^{-7}$ s. Computer simulations of Khare and Paulaitis[24] using transition-state theory reveals a very wide distribution of characteristic times of such flips that spans 21 decades, from 10^{11} to 10^{-10} s !

Apart from the investigation of the rotational mobility, local translational mobility has been studied in the very detailed quasielastic neutron scattering experiments of Kanaya et al.,[5] in the very broad temperature range of 21−475 K covering the glass transition temperature. In the time dependence of the mean-square proton translational displacements two distinct regimes were found: the short time regime for times $t < 5$ ps

* To whom correspondence should be addressed. E-mail address: a.v.lyulin@tue.nl.
† Technische Universiteit Eindhoven.
‡ Institute of Mathematical Problems of Biology.

10.1021/ma0212285 CCC: $22.00
Published on Web 11/08/2002

associated with a segment motion in the cage formed by the neighboring segments, and some slower regime as expected for the Rouse behavior. The coupling model (CM) of León, Ngai, and Roland[11] provides an interpretation of the existence of two different regimes of diffusion. According to CM model, intermolecular interactions only become important beyond a temperature-independent crossover time, t_c. For $t < t_c$, the molecular units relax independently of each other. At longer times intermolecular interactions slow the relaxation.

In contrast to the extensive experimental data, dynamic computer simulation studies of PS are rather scarce. Conformational properties of polystyrene (PS) have been studied in detail with molecular dynamics (MD) computer simulations by Roe et al.,[17,18] by Han and Boyd,[19] and by Ayyagari et al.[20] Main attention has been paid to the investigation of intermolecular statistical correlations of backbone atoms and mutual orientations of phenyl side groups. Roe[18] also studied short-time translational mobility in the vicinity of T_g. He showed that the mean-square translational displacements of the monomers reveal two dynamical processes: first a diffusive regime (for times less than 1 ps) and then a much slower subdiffusive process above 1 ps that is frozen in the glassy state (the cage effect). Qualitatively his results are in agreement with experimental finding of Kanaya et al.[5] These findings have been recently confirmed by more extensive MD simulations of Lyulin and Michels.[25,26]

Tremendous slowing down of the dynamic relaxation in polymer melts approaching the glass transition has been a subject of different theoretical considerations. Gotlib[34] discussed the dynamic model of α- and β-relaxations in which every chain element has two possible steady states, either the immobile "solidlike" state with strong intermolecular bonding or the mobile "liquidlike" state. In the high-temperature region only one $\alpha\beta$-process is active. For the low-temperature range when temperature becomes smaller than some characteristic temperature T^*, the theory[34] predicts a splitting of the $\alpha\beta$-process—the low-frequency branch (α-relaxation) and the high-frequency (or low temperature) β-relaxation branch. At $T < T_g$ the characteristic times of the α-relaxation become larger than characteristic times of usual experimental methods.

Increasing of the relaxation times by many orders of magnitude when approaching the glass transition is reasonably well described in general by the mode-coupling theory (MCT) of supercooled liquids.[27−32] The ideal form of MCT predicts a dynamical critical temperature T_c at which the molecules become permanently trapped in some cage formed by their almost frozen neighbors.

The general aim of our studies is to understand the differences in local segmental dynamics in different amorphous polymer melts above and below the glass transition by computer simulation, and to make the connection with chemical structure. In our previous study[25,26] molecular-dynamics simulations of amorphous atactic PS have been performed for chains up to 320 monomer units in a temperature range from 100 to 600 K and in a broad pressure range, from 0.1 to 1000 MPa, to validate the use of the model for description of the configurational and local dynamical properties of undercooled polymer melts. It was shown that the MD-determined specific-volume vs temperature curves are in a good agreement with experimental PVT data[35] at different values of applied pressure. The value of the MD-determined glass-transition temperature, $T_g = 370 \pm 5$ K, is in a very good agreement with the experimentally observed results. The long-time asymptotic slope of mean-square translational displacements of different segments in the main chain and in the phenyl groups is close to 0.6 at $T > T_g$, showing diffusive behavior. Temperature dependencies of the relaxation times for the Legendre polynomials of the first and second order have been found to be well described by the empirical Vogel−Fulcher law.[23]

The present paper serves as a logical continuation of previous studies;[18,25,26] the emphasis is now on the analysis of local translational and orientational mobility for a realistic model amorphous polymer melt and on comparison with the predictions of modern mode-coupling theory. We intend to check the coupling of the side groups and backbone relaxation found experimentally[9,10] by direct computer simulation in the broad temperature range below and above the glass transition.

For some low temperatures we thereby performed more simulations and managed to increase the simulated times up to 0.1 μs. The details of the simulation are presented in section 2. The results on local translational mobility, including the time dependence of the coherent intermediate scattering function, on conformational transitions and on local rotational mobility are discussed and analyzed in section 3. For the first time a universal translational and orientational activated behavior with similar activation energies is manifested at $T < T_g$, both for the backbone segments and side groups. In addition a universal algebraic T dependence of the characteristic relaxational times at $T > T_g$ has been obtained, in agreement with the predictions of MCT. These and other main conclusions are summarized in section 4.

2. Simulation Details

The united-atom model of PS of our previous study[25,26] is explored also in the present paper. The model consists of a single polymer chain of $N_p = 80$ monomers (molecular weight ∼ 9000), and its periodic images were generated by periodic boundary conditions. The stereochemic configurations of the aromatic groups were generated at random so that the ratio of number of *meso* to number of *racemic* dyads was near unity. The interaction potential has the following general form:

$$U = \sum_{|i-j|\le 3} \epsilon[(r_0/r_{ij})^{12} - 2(r_0/r_{ij})^6] + \sum_k k_\theta(\theta_k - \theta_0)^2 + \sum_l k_\varphi(1 - \cos 3\varphi_l) + \sum_m k_\chi \cos^2(\chi_m - \chi_0) + \sum_n k_\psi {\psi_n}^2 + \sum_{k_{arom}} \hat{k}_\theta(\theta_{k arom} - \hat{\theta}_0)^2 + \sum_{i_{arom}} \hat{k}_\varphi(1 + \cos 2\varphi_{i arom}) + U_{imp}$$

The following contributions to the force field have been considered: nonbonded interactions (∼ϵ) between all united atoms three or more bonds apart; bending potential (∼k_θ, $\hat{k}_\theta$) for all bond angles including those in the phenyl rings; torsional potential (∼k_φ) for the backbone; torsional potential (∼k_χ) for the phenyl-ring torsions; phenyl-ring (∼k_ψ) out-of-plane bending potential; torsional potential (∼$\hat{k}_\varphi$) about the $-C_{arom}-C_{arom}-$ bond; improper-torsion potential U_{imp}.

For the detailed forms of the potential contributions and the values of the potential constants we refer to ref 25.

For numerical expediency, the term for bond-stretching contributions is excluded from the interaction potential. The length of all valence bonds has been constrained by the SHAKE iterative procedure,[36] with a relative tolerance of 10^{-6}. Some runs have been performed for the model with flexible bonds; a harmonic spring in the force field with spring constant $k_b = 320$ kcal/mol has then been used for all bonds.

The leapfrog variant of the velocity Verlet algorithm[37] has been used to integrate the Newtonian equations of motion. For the present calculations well-equilibrated initial structures have been taken from the previous study.[25] To check the quality of equilibration, some runs have been performed using initial structures generated by the MSI Materials Studio Amorphous Cell interface.[38] For the model with flexible bonds the computations have been conducted with the help of a modified PUMA MD program[39] using the same force field (except for the additional harmonic term describing bond stretching). A collisional thermostat[39] and the Berendsen barostat[37] were used to keep the system at prescribed temperatures and pressures. The calculated final conformational properties and final densities were identical to those produced earlier.[25]

The production runs have been performed by NVE MD with the integration step of $\Delta t = 2-2.5$ fs. In the case of flexible bonds the integration time step was reduced to $\Delta t = 1$ fs. In all cases the length of these runs was from 10 to 30 ns. At $T = 270$ K, very deep in the glassy state, the length of the production run was about 100 ns.

3. Results and Discussion

A. Local Translational Mobility. The time scale of our typical computer experiment is rather small to obtain any noticeable displacement of a chain as a whole. Nevertheless, individual chain beads are quite mobile, even in the vicinity of T_g. Local translational mobility has been studied by measuring the mean-square translational displacements of individual beads in the main chain and in the side phenyl groups, Figure 1. The time dependence of these displacements have already been discussed in ref 25.

In the present paper, we intend to show that for our realistic polymer melt it can be understood within the framework of MCT.

At very small times ($t < 1-3$ ps) the regime of free monomer diffusion, with a slope of about 1, is seen. In a high-temperature melt, when $T \gg T_g$, this regime changes into a second diffusive regime, with the slope $\alpha \sim 0.54$, which confirms a well-known prediction for the Rouse chain. Actually the slope is slightly larger than the Rouse exponent 0.5, but this difference has been explained by the rather short chain length.[25] The time of the first free diffusive regime, with slope of about unity, should be proportional to the minimum Rouse relaxation time of the polymer chain, $\tau \sim t_{min} \sim \zeta/k_B T$, where ζ is the characteristic friction coefficient of the bead. With decreasing the temperature the motion of the chain bead is becoming more and more restricted: the onset of the second diffusion with the characteristic slope $\alpha \sim 0.54$ is preceded by some plateau. This plateau is connected with the cage effect, whereby very restricted local motions occur in the cage formed by surrounding monomers. The plateau is seen even at $T = 400$ K $> T_g = 373$ K, Figure 1a, meaning that some

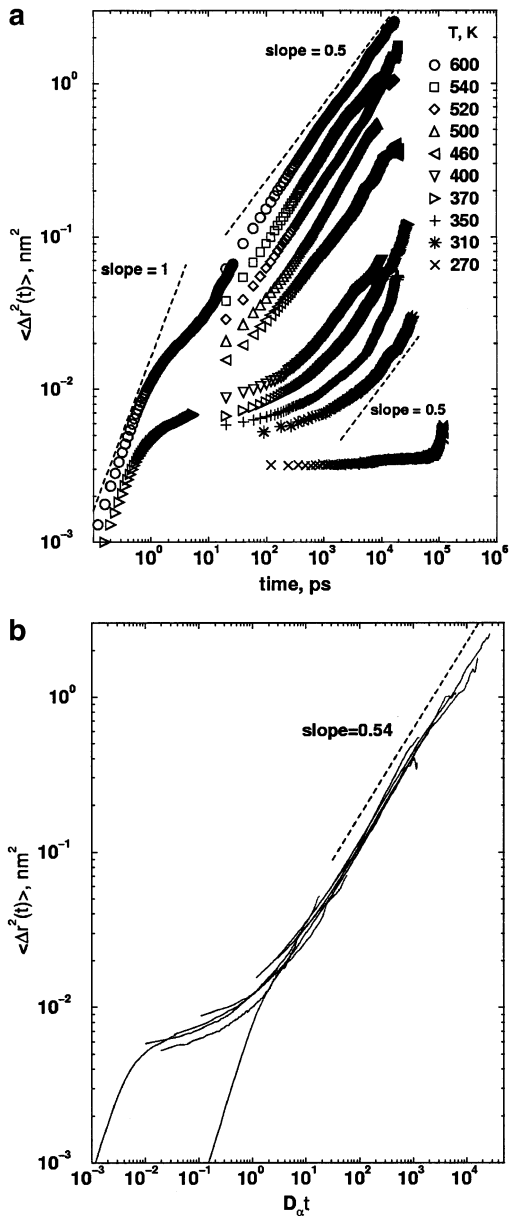

Figure 1. (a) Mean-square translational displacement of the average bead in the backbone at different temperatures. A diffusive regime with a slope close to 1 is observed for all temperatures up to $t = 3$ps. An asymptotic slope of ~0.54 is confirmed for temperatures close to T_g and higher. Crossover between these two regimes is a manifestation of the cage effect when the motion of chain monomers is restricted to some cage formed by the almost frozen neighborhood. Mean-square displacements for the phenyl groups show qualitatively the same behavior. (b) Mean-square displacement as a function of $D_\alpha t$ for each of the same temperatures as in part a. An asymptotic slope of 0.54 is shown by the dashed line.

cages are formed already in the melt. Qualitatively the same picture is valid for the motion of the individual phenyl side groups. At very low temperature, $T = 270$ K, the plateau is extended up to 0.1 μs whereupon the onset of the second diffusion is observed.

As suggested by van Zon and de Leeuw in their study of a model polymer melt without chemical details,[27] the idealized MCT for the translational α-relaxation may apply, which predicts that the final parts of the curves in Figure 1a can be fitted with the power law

$$\langle \Delta r^2(t) \rangle \sim (D_\alpha t)^\alpha \qquad (1)$$

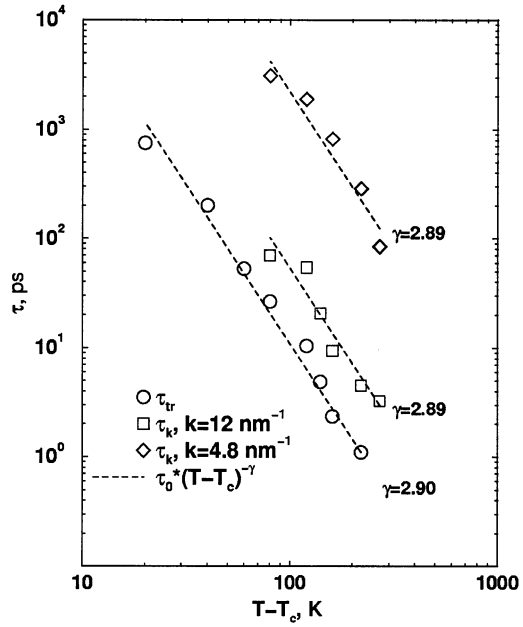

Figure 2. Temperature dependence of the translational relaxation times $\tau_{tr} = D_\alpha^{-1}$, eq 1, and τ_k, eq 6, for $k = 4.8$ and 12 nm^{-1}. Straight lines are fits according to eq 2 using $T_c = 380$ K.

where D_α is a diffusion constant in the regime of the Rouse diffusion. Averaging the exponents α for different temperatures gives $\alpha = 0.54 \pm 0.04$. The mean-square displacements are plotted as functions of $D_\alpha t$ at different temperatures in Figure 1b, showing this scaling behavior. According to the MC*T* the characteristic time of the α-relaxation, $\tau_{tr} = D_\alpha^{-1}$, algebraically diverges at some critical temperature T_c just above T_g:

$$\tau_{tr} = \frac{\tau_0}{(T - T_c)^\gamma} \tag{2}$$

Different exponents γ have been obtained in some previous simulations.[27−29] Using the simple bead−spring model Bennemann et al.[28,29] found $\gamma = 2.1-2.3$. For a model polymer with angle and torsion potentials, van Zon and de Leeuw[27] obtained $\gamma = 2.85$. Fitting with the straight line in Figure 2, we find that the power law (2) holds for few orders of magnitude and gives $T_c = 380 \pm 5$ K and $\gamma = 2.90 \pm 0.05$. This value of T_c is somewhat higher than the observed glass transition temperature $T_g \sim 370$ K, as predicted by MCT. The value of γ is in a very good agreement with the value of $\gamma = 2.85$ obtained by van Zon and de Leeuw[27] for the model polymer melt. The larger value of γ as compared to the results of Bennemann et al.[28,29] shows the influence of intramolecular interactions on the slowing down of dynamics in the vicinity of the glass transition.

The temperature dependence of $\tau_{tr} = D_\alpha^{-1}$ is for the full temperature range shown in Figure 3; as already mentioned at $T > T_g$, this dependence is well described by MCT (solid lines in Figure 3). At $T < T_g$, clearly different behavior is observed for the onset of the second diffusion regime; a simple activation law is used to fit the data for both the main-chain and side-group translational-diffusion times (dashed lines in Figure 3)

$$\tau_{tr} \sim \exp(E_a/k_B T) \tag{3}$$

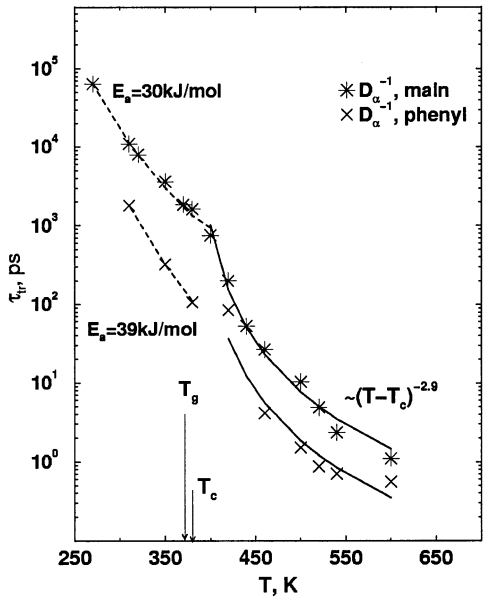

Figure 3. Temperature dependence of the translational relaxation times $\tau_{tr} = D_\alpha^{-1}$ both for the beads in the main chain and in the side group. Solid line is the MCT-based fit, eq 2. Dashed line is the fit with the simple activation law, eq 3.

This gives for the activation energy the values $E_a \sim 30$ kJ/mol (main chain) and $E_a \sim 39$ kJ/mol (phenyl group). We will compare these data on the translational sub-T_g relaxation with the data on rotational mobility in section D.

B. Coherent Intermediate Scattering Function. As in ref 30, the coherent intermediate scattering function of the PS melt is defined by

$$F(k,t) = S(k,t)/S(k) \tag{4}$$

where $S(k)$ is the static structure factor and $S(k,t)$ is defined as

$$S(k,t) = \frac{1}{N}\left\langle \sum_{i,j=1}^{N} \exp\{i\mathbf{q}[\mathbf{r}_i(t) - \mathbf{r}_j(0)]\} \right\rangle \tag{5}$$

$\mathbf{r}_i(t)$ is the position of the ith monomer at time t and $\langle\cdot\rangle$ denotes the usual canonical ensemble average. Aichele and Baschnagel[30] established that for a bead−spring model the temperature dependence of the α-relaxation times in the intermediate scattering function is well described by a power law in agreement with MCT. This observation is checked here for the realistic model of a polymer melt. The set of k values for which the scattering functions were calculated is from 4 to 29 nm^{-1} and is in the range $2\pi/R_g \le k \le 2\pi/l_b$, where R_g is the average radius of gyration and l_b is the bond length. A typical result for $k = 12$ nm^{-1} is shown in Figure 4 for the temperatures above the glass transition. Typical behavior of glass forming liquids is reproduced: a fast process for times $t < 2-3$ ps, followed by a plateau due to the cage effect, and finally the α-relaxation. Usually the fast process is associated with the so-called β-relaxation. With the time resolution used in the present simulations, it was not possible to study this initial relaxation process with sufficient precision. Instead, the main attention has been paid to the long-time α-relaxation. The relaxation times τ_k in the α-regime are obtained by using the Kohlraush−Williams−Watts (KWW) stretched exponent as the fit function:

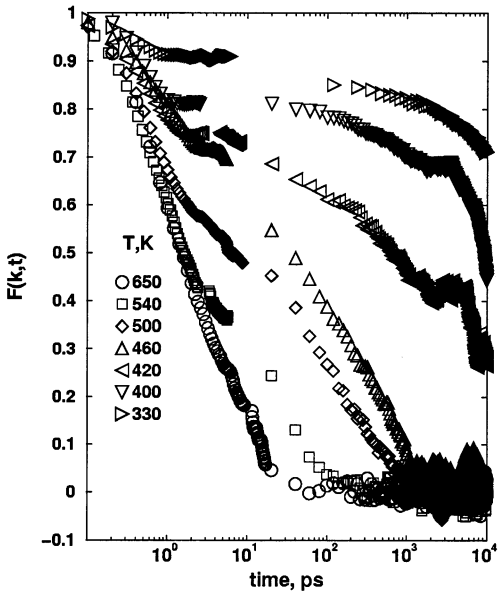

Figure 4. Coherent intermediate scattering function, eq 4, at $k = 12$ nm^{-1}, for temperatures $T > T_g$.

$$F(k,t) = \exp(-(t/\tau_k)^{\beta}) \quad (6)$$

The fitted times τ_k are plotted in Figure 2 as a function of temperature at different values of k. For $k \to 0$, the exponent β is getting closer to the value of the exponent α from eq 1, as it should be: using the Gaussian approximation in the region of small k, it is easy to see that

$$F(k,t) = \exp\left(-\frac{k^2}{6}\langle\Delta r^2(t)\rangle\right) = \exp\left(-\frac{k^2}{6}(t/\tau_{tr})^{\alpha}\right) \quad (7)$$

As k is increased, the values of β are seen to decrease from $\beta \sim 0.54$ to $\beta \sim 0.46$.

The temperature dependence of the times τ_k for different values of k is well reproduced by the same algebraic form (eq 2), with a critical temperature $T_c = 380 \pm 5$ K and exponent $\gamma = 2.89 \pm 0.05$, the same as for the characteristic time of the α-relaxation, τ_{tr}. This observation agrees with the findings of van Zon and de Leeuw.[27]

C. Conformational Transitions. We start the investigation of the orientational relaxation behavior with the study of conformational transitions and torsional-angle mobility. Both for the torsional angle in the main chain, φ_{main}, and for the angle of rotation of the phenyl group around the $C_{aliphatic}-C_{aromatic}$ bond, φ_{phe}, the temperature dependence of the mean-square angular displacement is shown in Figure 5. Some similarities with the translational mobility, Figure 1a, can already be noticed. At small times, $t < 1$ ps, the slope in the log−log time dependence for the main-chain angle φ_{main} is very close to unity, indicating free rotational diffusive behavior. At large times, the final slope of these dependencies should also be close to unity, but the time of the simulation is not long enough, and even at the rather high temperature $T = 600$ K the slope is approaching 0.5 at $t > 200$ ps. For the phenyl groups the final slope is close to unity for times $t > 300$ ps. At low temperature, $T < T_g$, the torsional mobility, just as the translational one, is almost frozen both for the main chain and side groups.

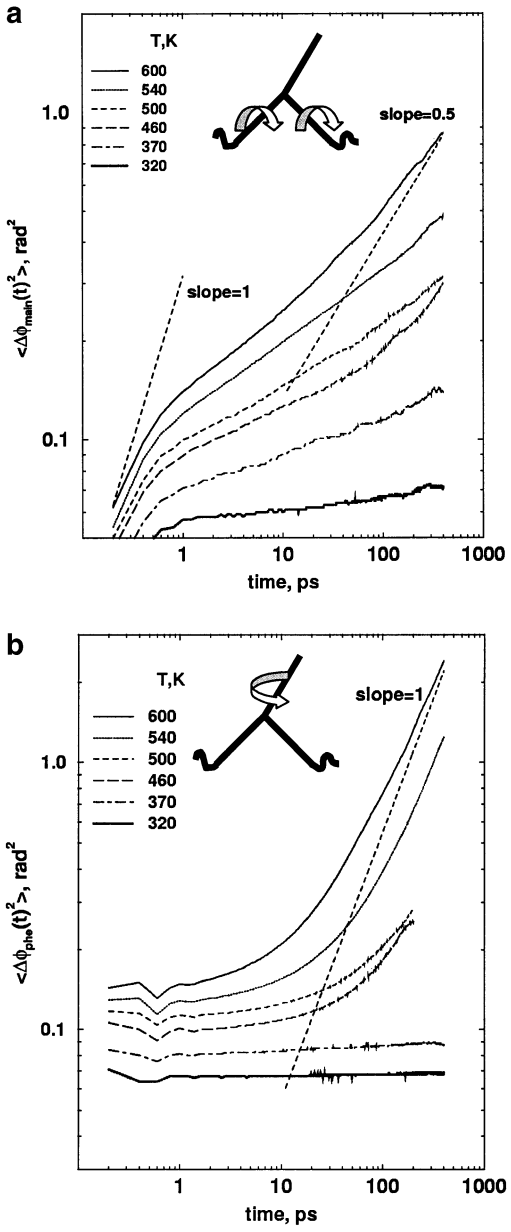

Figure 5. (a) Mean-square displacement of the average torsional angle in the middle of the backbone. (b) The same as in part a but for the side group in the middle of the chain.

At low temperature the main type of torsional motion is very fast libration around steady states, both for the main chain and side groups. At high-temperature some large-amplitude torsional displacements occur—180° flips of the phenyl rings and transitions between steady states both for the main-chain and phenyl-group torsional angles. Some of these conformational transitions are very correlated, with immediate back transitions from the new steady state to the previous one. The decrease in the value of the mean-square torsional displacement of phenyl groups which is seen at $t \sim 0.5$ ps in Figure 5b can be explained by these immediate back transitions.

Distribution functions of the average torsion angles φ_{main} and φ_{phe} in the middle region of the chain (first 10 torsional angles from the both chain ends are not taken into account for this analysis) are shown in Figure 6. Values of $\varphi_{phe} = 90°$ and $\varphi_{phe} = 270°$ would correspond to the orientation of the phenyl-ring plane perpendicular to the trans-zigzag plane of the backbone. Such a

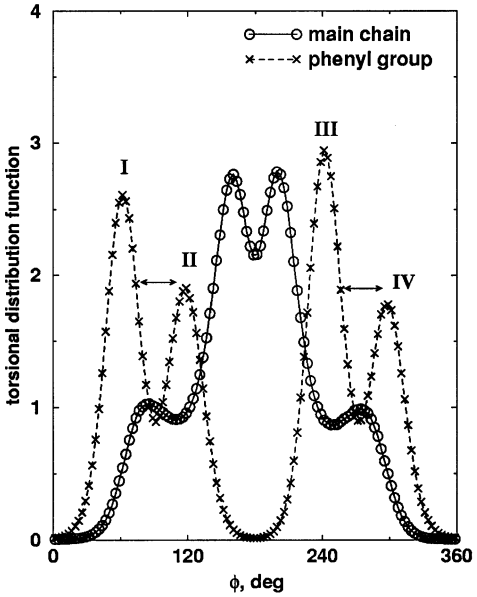

Figure 6. Distribution function of two types of dihedrals, in the main chain and in the side groups. Transitions I ↔ II and III ↔ IV contribute to the relaxation of the $P_{1,2}$ ACFs for the phenyl side groups.

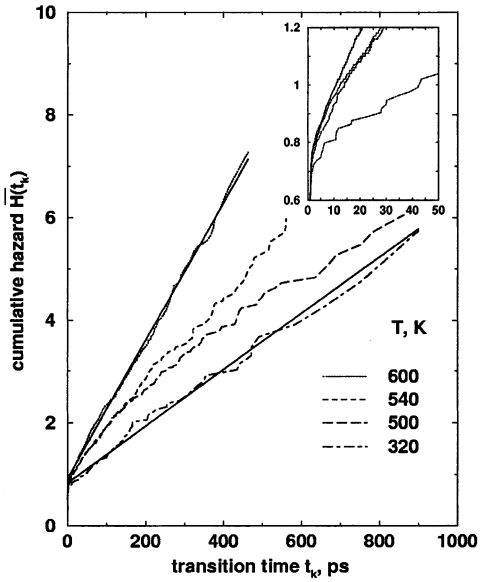

Figure 7. Hazard plots of the times of transitions between different conformational states of the phenyl groups. The initial part of cumulative hazard is shown in the inset. Solid lines represent the fits to eq 10.

situation is realized in the absence of the excluded-volume interactions, when the appropriate terms in the force field are switched off. The actual angle between two planes, $\varphi = 90° \pm \Delta\varphi$, where $\Delta\varphi \approx 30°$, is a result of the steric interactions between united atoms of the adjacent side groups. According to Figure 6, two mechanisms of orientational mobility of phenyl groups can be proposed: low-amplitude transitions between steady states I and II and between III and IV (see Figure 6), in which the orientation of the phenyl-ring plane with respect to the backbone does not change essentially; large-amplitude transitions I ↔ III, II ↔ IV (ring π-flips) and II ↔ III, I ↔ IV.

To have some insight into both types of transitions for the phenyl groups we use a technique proposed by Helfand[40] in his study of conformational transitions in a model solution of polyethylene, which is briefly explained here. At the beginning of a simulation run a clock is set to zero. The number of time steps required for a transition (for any phenyl-ring torsional angle to reach the bottom of any potential well) is then counted. The clock is reset to zero and the next transition time is measured. So all transition times are the first-passage times from one potential minimum to the other. As a result a set of n transition times is obtained. These are arranged in ascending order, $t_{(1)} < t_{(2)} < \ldots < t_{(n)}$. Following Helfand, we use the methods of hazard graphing from reliability analysis[41] to analyze these times.

Let us define the hazard rate $h(t)$ such that $h(t)\,\mathrm{d}t$ is the probability that a torsional angle which has survived a time t since the last transition will undergo a transition at a time between t and $t + \mathrm{d}t$. The cumulative hazard is defined as

$$H(t) = \int_0^t h(t')\,\mathrm{d}t' \tag{8}$$

The expectation value $\bar{H}(t_k)$ of the cumulative hazard at the time of the kth ordered transition is found to be[40,41]

$$\bar{H}(t_k) = \sum_{l=0}^{k-1} \frac{1}{n-l} \tag{9}$$

and, following Helfand, could be fitted by

$$\bar{H}(t) = t/\tau + v\sigma[1 - \exp(-t/\sigma)] \tag{10}$$

The first term in (10) corresponds to the contribution from the independent transitions with $1/\tau$ as an average rate of transition, the second term describes forced backreactions. The cumulative hazards in (9) and its fit in (10) (the two solid lines in Figure 7) at different temperatures are graphically shown in Figure 7. For $\sigma \ll 1/\tau$, one can say that a fraction

$$c \sim 1 - \exp(-v\sigma) \tag{11}$$

undergoes a transition via an enhanced mechanism following the initial transition. The initial part of the cumulative hazard is shown as an inset in Figure 7. Indeed, quite a big correlation (up to $c = 70\%$) of transitions is seen. These transitions are rather fast, with an average time of about $\sigma = 1$ ps. The asymptotic slope of cumulative hazard plots gives an average time $\tau \sim 200$ ps between such fast transitions. The temperature dependence of these average times is very weak and is shown in Figure 9a (crosses). When analyzing the transition times set further, fast transitions as well as quite numerous transitions I ↔ II and III ↔ IV were removed. Only few real phenyl ring flips per simulation run (10−100 ns) have been counted, and only at rather high temperature. No transitions between the steady states II and III and between I and IV were found. We can conclude that only low-amplitude fast librations of phenyl rings contribute to both their translational and orientational relaxations. The coupling of these relaxations with the mobility of the main-chain segments is discussed in section D.

D. Local Orientational Mobility. To have insight into possible common mechanisms of the different types of segmental mobility (translational and rotational) and in order to compare the results with the predictions of

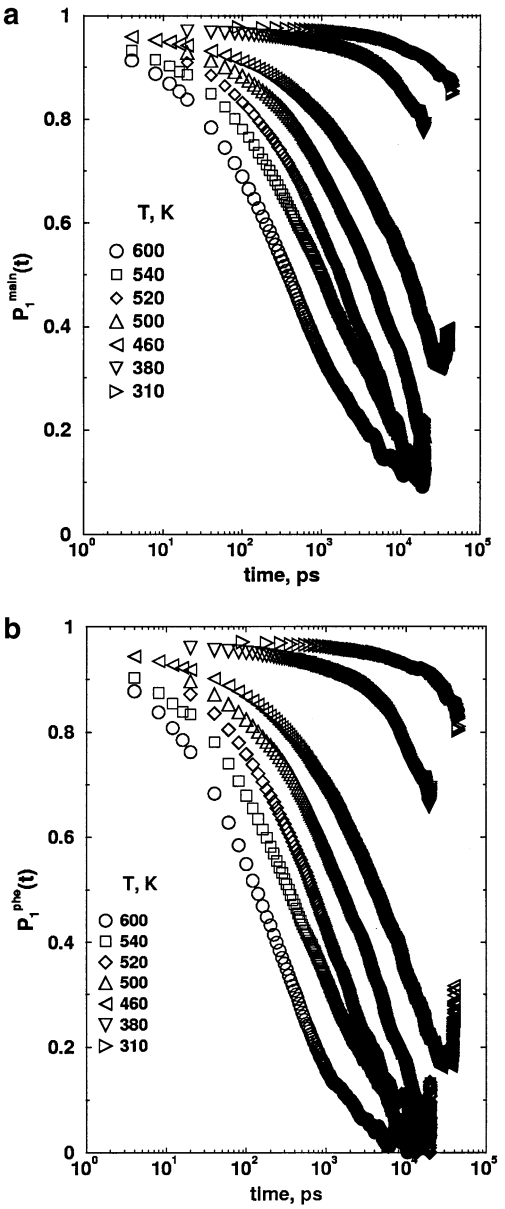

Figure 8. (a) Temperature dependence of the P_1 ACF for the average bond in the middle of the main chain. (b) Same plot, but for the average side group in the middle of the chain.

MCT, the local orientational mobility has been studied with the help of Legendre polynomials of the first and second order (autocorrelation functions, ACFs)

$$P_1(t) = \langle \mathbf{b}(0)\mathbf{b}(t)\rangle$$
$$P_2(t) = \langle {}^3/_2(\mathbf{b}(0)\mathbf{b}(t))^2 - {}^1/_2\rangle \qquad (12)$$

where **b** is the unit vector directed along the main-chain bond or along the phenyl side group, averaged for the middle of the chain; the brackets denote an ensemble averaging. A decrease of temperature leads to a pronounced slowing down of the orientational mobility both for the P_1 and P_2 ACFs. The orientational relaxation for the bond in the middle of the chain is almost frozen in the vicinity of T_g, Figure 8a,b. The phenyl side groups are more mobile as compared to the bonds in the main chain at the same value of temperature.

As in the case of the intermediate scattering function, KWW-stretched exponents (eq 6) have been used to fit the P_1 and P_2 ACFs at different values of temperature

$$P_{1,2}(t) = \exp(-(t/\tau_{1,2})^{\beta}) \qquad (13)$$

where $\tau_{1,2}$ is the characteristic relaxation time and β is the parameter effectively taking into account the non-exponential nature of the relaxation process. At low temperatures, $T < T_g$, the relaxation of P_1 and P_2 ACFs is far from complete, but nevertheless, the fits are good and allow us to determine relaxation times which are much larger than the actual length of the simulation run. The temperature dependence of the relaxation times $\tau_{1,2}$ is shown in Figure 9a. In the melt, when $T > T_g$, the T dependence is clearly non-Arrhenius; its shape is similar to the experimentally observed α-process. First of all, the Vogel−Fulcher empirical equation has been used to fit the data in Figure 9a

$$\tau_{1,2}{}^{-1} \sim \exp(-E_a/k_B(T - T_0)) \qquad (14)$$

From this fit quite similar results have been obtained, $E_a \sim 10$ kJ/mol and $T_0 \sim 300$ K (essentially lower than T_g), for the P_1 and P_2 ACFs, both for the main chain and side groups. At low temperature, $T < T_g$, the T dependence of the relaxation times shows different behavior and is described as a simple activation process with an activation energy (averaged for all four data sets in Figure 9a) $E_a = 31$ kJ/mol. This value of the activation energy is close to the value $E_a \sim 30$ kJ/mol observed earlier for the onset of the second translational diffusion regime at $T < T_g$, associated with the escape from the particle's cage. The results of the MD simulation of Boyd and Boyd[22] for the T dependence of the relaxation times of individual dipoles in the main chain of amorphous poly(ethyleneterephthalate), explained in ref 22 as a single (merged α and β) process, are quite close to the present simulation data.

We also have tried to fit the temperature dependence of the relaxation times $\tau_{1,2}$ at $T > T_g$ with the power-law fits of (2) predicted by MCT for the α-relaxation, Figure 9b. First of all, the fits give the same value of the critical temperature, $T_c = 380$ K, as in the case of the translational diffusion and intermediate scattering function. Second, the average exponent $\gamma = 2.88$ is very close to the values of 2.90 for τ_{tr} and 2.89 for τ_k.

To complete the picture we plot the $P_{1,2}$ orientational relaxation times as functions of temperature, Figure 9c, as we did earlier for translational relaxation times $\tau_{tr} = D_\alpha{}^{-1}$ in Figure 3. Qualitatively the picture of reorientational relaxation is very similar to the translational relaxation: the T dependence of the characteristic relaxation times is changed from the algebraic dependence described by MCT, eq 2, to the simple activated process, eq 3, both for the translational and orientational relaxation. The values of the critical temperature T_c, power γ, and activation energy E_a are very close for both types of mobility, orientational and translational. We can generally conclude here that the predictions of MCT hold at $T > T_g$ for both types of mobility. Because of the scattering of the data, it is difficult to make any precise conclusions about the temperature dependence of the KWW parameter β.

E. Distribution of Relaxation Times and Cross-Correlation. In the previous section the orientational ACFs were characterized by some average characteristic relaxation time. Alternatively, each orientational ACF can be analyzed using the CONTIN[42,43] method and can be represented as

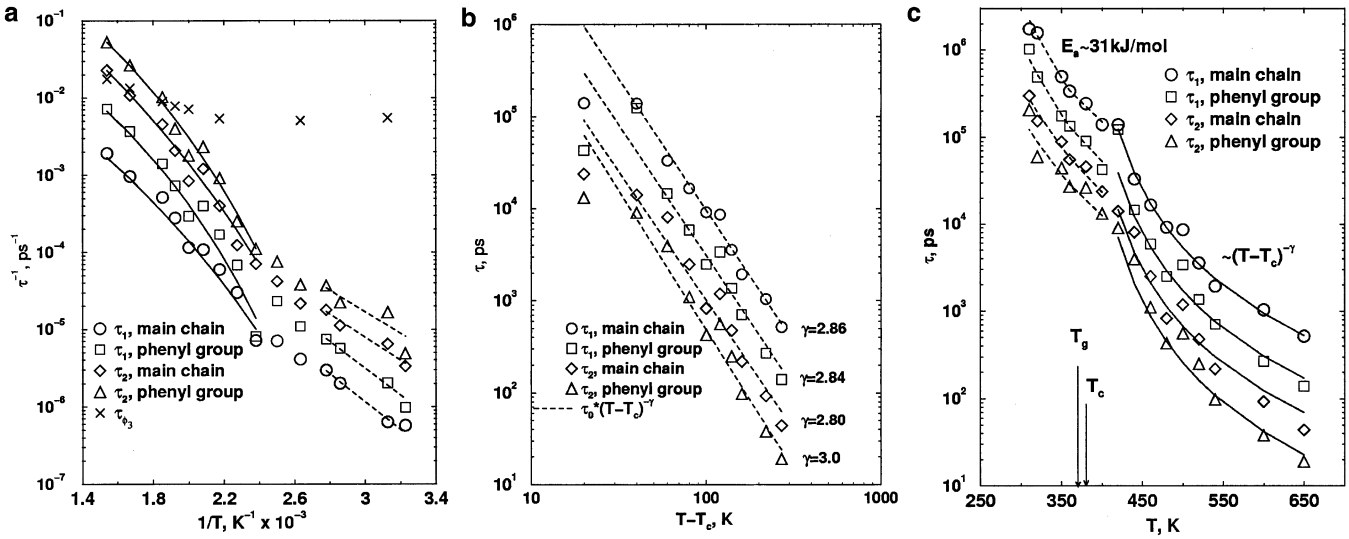

Figure 9. (a) Temperature dependence of the relaxation times $\tau_{1,2}$ of the $P_{1,2}$ ACFs. Solid lines are Vogel−Fulcher fits, eq 14, to the data at $T > T_g$. Dashed lines are fits with the simple activation law at $T < T_g$. Crosses represent the data of the hazard plot analysis of the fast librations of phenyl rings. (b) Temperature dependence of the relaxation times $\tau_{1,2}$ of the $P_{1,2}$ ACFs at $T > T_g$. Straight lines are fits according to eq 2 using $T_c = 380$ K. (c) Temperature dependence of the relaxation times $\tau_{1,2}$ of the $P_{1,2}$ ACFs both for the main chain and the side group. Solid lines are the MCT-based fits, eq 2. Dashed lines are the fits with the simple activation law.

$$ACF(t) = \int_{-\infty}^{+\infty} F(\ln \tau) \exp(-t/\tau)\, d(\ln \tau) \qquad (15)$$

where $F(\ln \tau)$ is a normalized distribution function of relaxation times. The inversion of eq 15 is an ill-posed problem in that there exists a large number of possible solutions all of which fit the data to within statistical error. A CONTIN general-purpose constrained-regularization method[42,43] finds the simplest (most parsimonious) solution that is consistent with the simulated ACFs. The problem is formulated as a weighted least-squares problem with an added quadratic form, the regularizor, which imposes parsimony (smoothness). A characteristic relaxation time for each process in the spectra can be associated with the corresponding peak in this distribution function. The distribution function of relaxation times for the P_2 ACF is shown in Figure 10a,b for the main-chain bond and phenyl groups, respectively. First of all, the distribution functions for the main-chain bond and side phenyl group qualitatively are very similar: at high temperature these functions are unimodal, with the location of the peak shifted toward larger times with decreasing temperature. The positions of the peaks correspond to the relaxation times of the α-process. At $T = 500$ K, the form of the distribution function is becoming bimodal, with one peak located at $\tau \sim 1$ ns and another corresponding to a very slow process at $\tau \sim 10^3$ ns. At $T = 400$ K analysis reveals a very broad distribution of relaxation times, which could be due to the merging of α- (main structural) relaxation and sub-T_g relaxation processes at this temperature. At lower temperatures, $T < T_g$, the distribution function again becomes unimodal, with a single peak at extremely large values of relaxation times, $\tau > 10^3$ ns, and with a weaker temperature dependence than above T_g; qualitatively, this should correspond to the previously discussed activated process, which in the present analysis turns out to announce itself already above T_g by an emerging second peak next to the α-relaxation.

The similar shapes of the distribution functions in Figure 10a,b show a strong coupling between motions of the backbone and side phenyl groups. To study this coupling in detail we calculated the following cross-correlation function:

$$C(t) = \frac{\langle (\mathbf{a}_i(0)\cdot\mathbf{b}_i(0))(\mathbf{a}_i(t)\cdot\mathbf{b}_i(t))\rangle}{\langle (\mathbf{a}_i\cdot\mathbf{b}_i)^2\rangle} \qquad (16)$$

where $\mathbf{a}_i = \mathbf{l}_i - \mathbf{l}_{i+1}$ ($\mathbf{l}_i$ is the unit vector along the bond in the backbone and $\mathbf{b}_i$ is the $C-C$ unit vector in the phenyl ring: see the inset of Figure 11b). These ACFs are shown in Figure 11a (solid lines) together with the ACFs for individual vectors **a** (dotted curves) and **b** (dashed curves) at different temperatures. The coupling is very strong (almost three decades in time) even at high temperatures, $T = 650$ K, and much longer than characteristic relaxation times (about 1 ns) of the relaxation of the individual vectors **a** and **b** at this temperature. In the glassy state, $T = 360$ K, the motions of the main chain and side groups are coupled in the whole region of simulated times, up to $t \sim 10^{-7}$s.

The steric hindrance due to the excluded-volume interactions is the main reason for the backbone-side-chain coupling. In Figure 11b, the cross-correlation function $C(t)$ together with the ACFs for individual backbone and side-group vectors are plotted for the PS melt at $T = 360$ K. In that case, the term in the force field describing the nonbonded interactions between all united atoms three or more bonds apart was switched off. In contrast to the results described earlier, the correlation of the orientational motions of the backbone and of the phenyl group disappears after $t \sim 40$ ps, only a factor of 4 above the relaxation time of the individual backbone and phenyl-group vectors at this temperature; at high temperature this time of the coupled motion becomes even smaller. This implies that the steric hindrance is the main reason for the strongly coupled motions of the side groups and the main chain.

4. Conclusions

Using the united atom (UA) model from our previous study,[25] we have investigated the local dynamical properties of an atactic-polystyrene melt in the vicinity

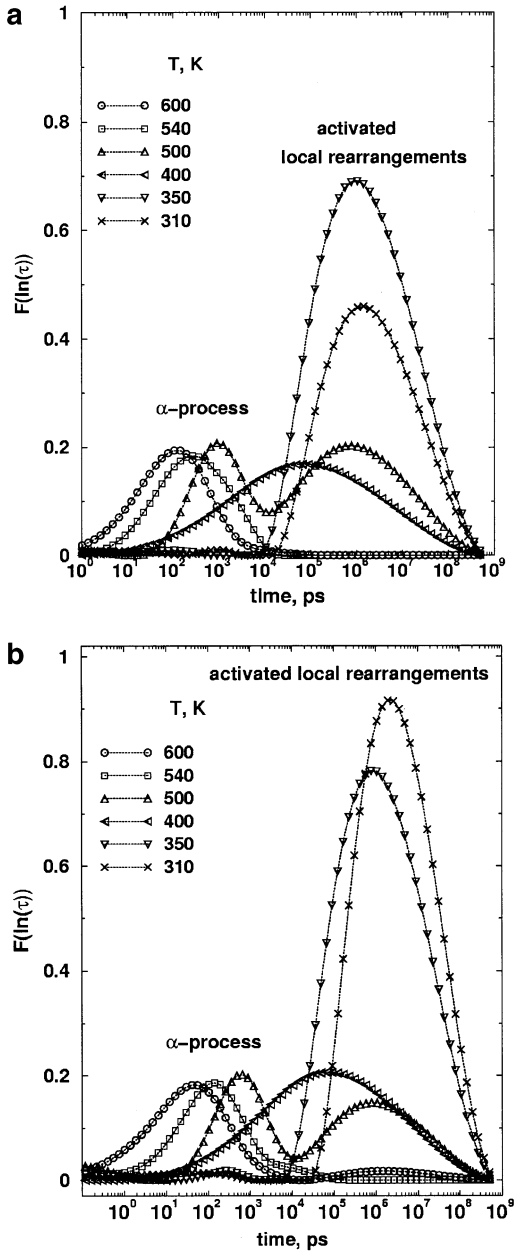

Figure 10. (a) Temperature dependence of the normalized distribution function of the relaxation times for the $P_2(t)$ ACF for the average bond in the middle of the backbone. Two peaks correspond to two different relaxation processes, diffusive and local activated rearrangement. (b) The same, but for the average phenyl side group in the middle of the chain.

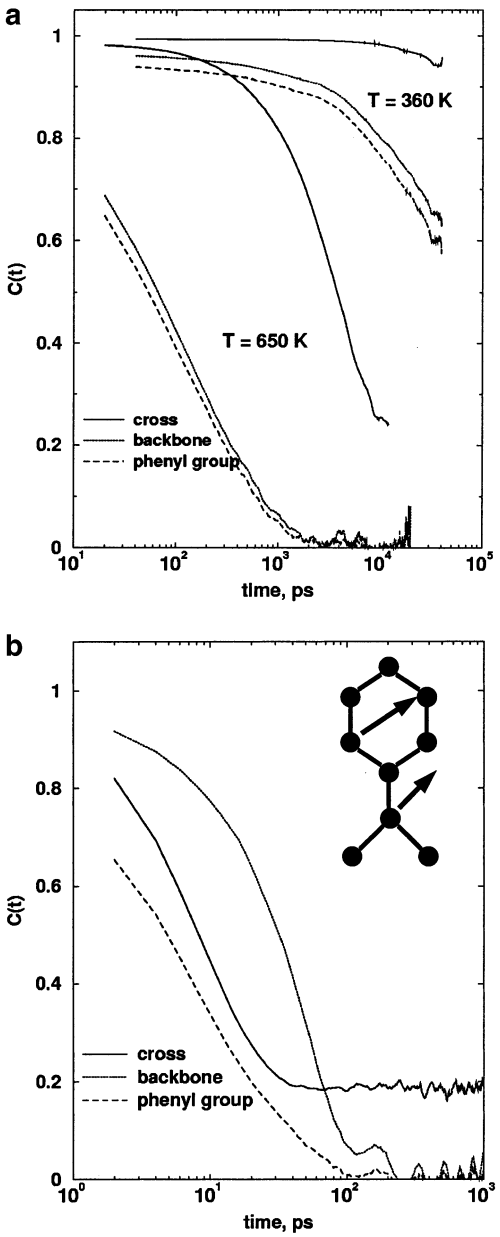

Figure 11. (a) Cross-correlation function, eq 16 (solid lines), and individual P_1 ACFs for the vectors **a** and **b** (see the inset in Figure 11b) at two different temperatures, above and below T_g. (b) Same as in part a but with the excluded-volume interactions switched off. Temperature is $T = 360$ K.

of the glass transition, $T_g \sim 370$ K. The UA model has a better performance in comparison with an explicit atom (EA) model. However, as shown by Smith and Yoon,[44] the results of the MD simulations of the local dynamical properties of *n*-tridecane melts using both the UA and the EA model could be different. Results of the present simulations are qualitatively in agreement with those produced for the EA model of the atactic PS melt with the help of the MSI Materials Studio software. Detailed simulations of much longer chains for both models of PS are necessary in order to make definite conclusions. These simulations as well as the results for the many-chain systems are the subjects of a future publication. The main attention in the present paper has been paid to the study of the possible universality of internal translational and orientational segmental mobility, including conformational transitions, and to comparison with the predictions of MCT. Translational mobility has been investigated by using the mean-square displacements of different beads and the coherent intermediate scattering function. The slowing down near T_g of the translational mobility of the monomers in the chain is mainly explained by the existence and diffusion of cages formed by their almost frozen neighborhood. A crossover between the first diffusive regime of free Brownian monomer motion to the motion hindered by the cage boundaries occurs at times of 1−3 ps, in good agreement with data from quasielastic neutron scattering experiments[5] and with the results of the previous simulations.[18] Onset of the second diffusion regime is associated with the escape of the particle from its cage. Analysis of the mean-square displacements at longer times reveals Rouse-like dynamics with an asymptotic power-law behavior $\langle \Delta r^2(t) \rangle \sim t^{0.54}$, both for

the main chain and the phenyl side groups. From the long-time asymptotics of the mean-square displacements the corresponding translational relaxation times $\tau_{tr} = D_\alpha^{-1}$ were defined. The temperature dependence of these times is described by a power law with the exponent $\gamma = 2.90$ and critical temperature $T_c = 380$ K at $T > T_g$ (α-relaxation regime) in good agreement with the predictions of the MCT. The relaxation times of the intermediate scattering function in the α-relaxation regime follow the same power-law behavior as τ_{tr}. At $T < T_g$ the temperature dependence of the characteristic "cage release" time is fitted by a simple activation law with the activation energy of about 30 kJ/mol for the main chain bonds and 39 kJ/mol for the phenyl groups.

The rotational mobility is investigated with the help of the time autocorrelation functions for the Legendre polynomials of the first and second order for unit vectors that characterize the directions of the main-chain bonds and phenyl side groups. In the vicinity of T_g the orientational relaxation as well as the translational one are almost frozen for both types of bonds. Nevertheless, the time dependences of ACFs are well described by the KWW stretched exponents, making it possible to obtain information about characteristic times far beyond the length of the present simulations. As in the case of the translational relaxation, similar non-Arrhenius T dependence of the relaxation times for the orientational α-relaxation at $T > T_g$ is well reproduced. The temperature dependence of the relaxation times of the α-relaxation process follows the same power law behavior as the translational relaxation times and intermediate scattering function. Distribution function of P_2 relaxation times is bimodal, with activated process announcing itself already at $T > T_g$. At $T < T_g$ the temperature dependence of the orientational relaxation times is close to the simple activation process, with the value of activation energy $E_a \sim 31$ kJ/mol, both for the main-chain bonds and for the side groups. Both translational and orientational mobility show strong coupling of the motions of the phenyl groups and the backbone in the broad range of temperatures due to the strong steric interactions. In summary, both translational and orientational segmental relaxation processes show similar behavior: algebraic slowing down at $T > T_g$ and activated rearrangements at much larger times at $T < T_g$.

Deep insight into the nature of different relaxation processes can be obtained with the help of investigation of conformational transitions. The study of the phase trajectories by using the Helfand hazard-plot analysis[40] shows that the majority of these transitions are highly correlated back transitions to the previous steady state. This type of motion is the main contribution to the relaxation of the P_1 and P_2 ACFs. At a rather high temperature ($T = 500-600$ K), we managed to notice only a few real phenyl-ring flips during 10−30 ns of simulation.

Acknowledgment. This work is the part of the research program of the Dutch Polymer Institute. Grateful acknowledgment is made to Prof. Yu. Gotlib (Institute of Macromolecular Compounds, St. Petersburg, Russia), Prof. J. J. M. Slot, and Dr. A. Stroeks (DSM Research, The Netherlands) for many useful discussions. N.K.B. acknowledges the financial support from the Nederlandse Organisatie voor Wetenschappelijk Onderzoek (NWO).

References and Notes

(1) Baccaredda, M.; Butta, E.; Frosini, V. *Polym. Lett.* **1965**, *3*, 189.
(2) Yano, O.; Wada, Y. *J. Polym. Sci. A* **1971**, *9*, 669.
(3) Beaume, F.; Brulé, B.; Halary, J.-L.; Lauprêtre, F.; Monnerie, L. *Polymer* **2000**, *41*, 5451.
(4) Zajıc, W.; Gabryś, B.; Peiffer, D. G.; Adams, M. A. *Physica B* **1992**, *182*, 365.
(5) Kanaya, T.; Kawaguchi, T.; Kaji, K. *J. Chem. Phys.* **1996**, *104*, 3841.
(6) Fukao, K.; Miyamoto, Y.; Miyaji, H. *J. Phys. Condens. Matter* **1991**, *3*, 5451.
(7) Fukao, K.; Mayamoto, Y. *Polymer* **1993**, *34*, 238.
(8) Fukao, K.; Miyamoto, Y. *J. Non-Cryst. Solids* **1994**, 172−174, 365.
(9) Mansour, A. A.; Junge, R.; Stoll, B.; Pechhold, W. *Colloid Polym. Sci.* **1992**, *270*, 325.
(10) Mansour, A. A.; Happ, E.; Wolf, T.; Stoll, B. *Colloid Polym. Sci.* **1994**, *272*, 894.
(11) León, C.; Ngai, K. L.; Roland, C. M. *J. Chem. Phys.* **1999**, *110*, 11585.
(12) Wübbenhorst, M.; de Rooij, A. L.; van Turnhout, J.; Tacx, J.; Mathot, V. *Colloid Polym. Sci.* **2001**, *279*, 525.
(13) Vol'kenstein, M. V.; Kol'tsov, A. I.; Khachaturov, A. S. *Vysokomol. Soedin. (Polym. Sci. USSR)* **1965**, *7*, 296.
(14) Connor, T. M. *J. Polym. Sci. A* **1970**, *8*, 191.
(15) Spiess, H. W. *Colloid Polym. Sci.* **1983**, *261*, 193.
(16) Kuebler, S. C.; Heuer, A.; Spiess, H. W. *Phys. Rev. E* **1997**, *56*, 741.
(17) Mondello, M.; et al. *Macromolecules* **1994**, *27*, 3566. Furuya, H.; et al. *Macromolecules* **1994**, *27*, 5674. Roe R. J.; et al. *Macromolecules* **1995**, *28*, 2807.
(18) Roe R. J. *J. Non-Cryst. Solids* **1998**, 235−237, 308.
(19) Han, J.; Boyd, R. H. *Polymer* **1996**, *37*, 1797.
(20) Ayyagari, C.; Bedrov, D.; Smith, G. *Macromolecules* **2000**, *33*, 6194.
(21) Yip, S.; Sylvester, M. F.; Argon, A. S. *Comput. Theor. Polym. Sci.* **2000**, *10*, 235.
(22) Boyd, S. U.; Boyd, R. H. *Macromolecules* **2001**, *34*, 7219.
(23) Karatasos, K.; Ryckaert, J.-P.; Ricciardi, R.; Laupretre, F. *Macromolecules* **2002**, *35*, 1451.
(24) Khare, R.; Paulaitis, M. E. *Macromolecules* **1995**, *28*, 4495.
(25) Lyulin, A. V.; Michels, M. A. J. *Macromolecules* **2002**, *35*, 1463.
(26) Lyulin, A. V.; Michels, M. A. J. *Comput. Phys. Commun.* **2002**, *147*, 298.
(27) van Zon, A.; de Leeuw, S. W. *Phys. Rev. E* **1999**, *60*, 6942.
(28) Bennemann, C.; Baschnagel, J.; Paul, W.; Binder, K. *Comput. Theor. Polym. Sci.* **1999**, *9*, 217.
(29) Bennemann, C.; Baschnagel, J.; Paul, W. *Eur. Phys. J. B* **1999**, *10*, 323.
(30) Aichele, M.; Baschnagel, J. *Eur. Phys. J. E* **2001**, *5*, 229.
(31) Aichele, M.; Baschnagel, J. *Eur. Phys. J. E* **2001**, *5*, 245.
(32) See Götze, W. in *Liquids, Freezing and Glass Transition*; Hansen, J. P., Levesque, D., Zinn-Justin, J., Eds.; Elsevier B. V.: Amsterdam, 1991.
(33) Ferry, J. D. *Viscoelastic Properties of Polymers*, 2nd ed.; J. Wiley: New York, 1970.
(34) Gotlib Yu. Ya. *J. Polym. Sci., Polym. Symp.* **1968**, *16*, 3365.
(35) Zoller, P.; Walsh D. J. *Standard Pressure−Volume−Temperature Data for Polymers*; Technomic: Lancaster, PA, 1995.
(36) Ciccotti, G.; Ferrario, M.; Ryckaert, J.-P. *Mol. Phys.* **1982**, *47*, 1253.
(37) Allen, M. P.; Tildesley, D. J. *Computer Simulation of Liquids*; Clarendon Press: Oxford, England, 1987.
(38) *Materials Studio Getting Started*; Molecular Simulations Inc.: San Diego, CA, 2000.
(39) Lemak, A. S.; Balabaev N. K. *J. Comput. Chem.*, **1996**, *17*, 1685.
(40) Helfand, E. *J. Chem. Phys.* **1978**, *69* 1010.
(41) Helfand, E. *J. Appl. Phys.* **1977**, *48*, 3251.
(42) Provencher, S.; Dovi, V. *J. Biochem. Biophys. Methods* **1979**, *1*, 313.
(43) Provencher, S. *Comput. Phys. Commun.* **1982**, *27*, 213.
(44) Smith, G. D.; Yoon, J. *J. Chem. Phys.* **1994**, *100*, 649.

MA0212285